Effect of Molecular Packing on Field-Effect Performance of Single Crystals of Thienyl-Substituted Pyrenes

Minoru Ashizawa,*[,†,‡] Koichi Yamada,[§] Atsuko Fukaya,[†] Reizo Kato,*[,†] Kouji Hara,[||] and Jun Takeya*[,||]

Condensed Molecular Materials Laboratory, RIKEN, 2-1, Hirosawa, Wako-shi, Saitama 351-0198, Japan, MSRL, CRIEPI, 2-11-1, Komae, Tokyo 201-8511, Japan, and Department of Chemistry, Graduate School of Science, Osaka University, Toyonaka 560-0043, Japan

Received December 8, 2007. Revised Manuscript Received May 20, 2008

A series of pyrene derivatives containing thienyl groups, **1**−**3**, has been prepared using the Suzuki coupling reaction. Recrystallization from solution and physical vapor transport (PVT) method afforded different types of crystals of **1**. From the mixture of isomers of **2**, the 1,8-isomer preferably crystallized from solution, whereas the 1,6-isomer crystal was obtained by the PVT method. Fabricating single-crystal-based field-effect transistors of the above compounds we directly compared the field-effect performance between the devices of the two isoforms of **1** and those of the two isomers of **2**. Though the overlap integrals were calculated to be only $\sim 10^{-3}$, the best hole mobility reached 0.02 $cm^2\ V^{-1}\ s^{-1}$ for one of the single crystals of **1**. Intriguingly, for both **1** and **2** only one type of the crystal shows the field-effect characteristics, indicating the significance of molecular packing even in the absence of band transport among the poorly coupled molecules. The estimated intermolecular overlap integrals for each compound also imply that the minimum overlap integral of $\sim 10^{-2}$ eV is required for detection of the field-effect characteristics.

Introduction

Organic semiconductors play the most essential part as active layers in organic field-effect transistors (OFETs). They have been intensively studied recently because of their unique advantages against conventional silicon-based FETs, including low fabrication cost, large area coverage, and mechanical flexibility.[1] During the past decade, significant progress has been achieved for the OFETs in both materials development and advanced fabrication techniques toward the industrial application.[2] Among them, a large amount of effort has been devoted to developing superior p-type organic semiconductors with high carrier mobilities when incorporated in the FET devices.[3] A mobility value as high as $\mu = 1.5\ cm^2\ V^{-1}\ s^{-1}$ is achieved for pentacene polycrystalline thin films on chemically modified surfaces of SiO_2/Si substrates,[4] and $\mu = 1.1\ cm^2\ V^{-1}\ s^{-1}$ is realized for alkyl-attached oligothiophene thin-film devices.[5] For recently developed single-crystal OFETs, the highest mobility for rubrene crystals reaches more than $\sim 30\ cm^2\ V^{-1}\ s^{-1}$, which surpasses even that of amorphous silicon FETs.[6]

For material design to improve the device performance, it is crucial to elucidate mechanisms to relate the microscopic molecular arrangement to the macroscopic electronic charge transport demonstrated in the FET performance. To make use of the full capability of the organic compounds, the

* To whom correspondence should be addressed. M.A.: phone, +81-48-467-9412; fax, +81-48-467-4661; e-mail: mashizawa@riken.jp. J.T.: phone, +81-6-6850-5398; fax, +81-6-6850-5398; e-mail, takeya@chem.sci.osaka-u.ac.jp.

[†] Condensed Molecular Materials Laboratory.

[‡] Current address: Department of Organic and Polymeric Materials, Tokyo Institute of Technology, 2-12-1 O-okayama, Meguro-ku 152-8552, Japan. Phone: +81-3-5734-2426. Fax: +81-3-5734-2876. E-mail: ashizawa.m.aa@m.titech.ac.jp.

[§] MSRL.

[||] Osaka University.

(1) (a) Dimitrakopoulos, C. D.; Mascaro, D. J. *Adv. Mater.* **2002**, *14*, 99. (b) Garnier, F.; Hajlaoui, R.; Yassar, A.; Srivastava, P. *Science* **1994**, *265*, 1684. (c) Bao, Z. *Adv. Mater.* **2000**, *12*, 227. (d) Horowitz, G. *J. Mater. Chem.* **1999**, *9*, 2021. (e) Horowitz, G. *Adv. Mater.* **1998**, *10*, 365. (f) In *Thin-Film Transistors*; Kagan, C. R., Andry, P., Eds.; Marcel Dekker: New York, 2003; p 377. (g) Briseno, A. L.; Tseng, R. J.; Ling, M.-M.; Falcao, E. H. L.; Yang, Y.; Wudl, F.; Bao, Z. *Adv. Mater.* **2006**, *18*, 2320.

(2) (a) Facchetti, A.; Mushrush, M.; Katz, H. E.; Marks, T. J. *Adv. Mater.* **2003**, *15*, 33. (b) Malanfant, P. R. L.; Dimitrakopoulos, C. D.; Gelorme, J. D.; Kosbar, L. L.; Graham, T. O. *Appl. Phys. Lett.* **2002**, *80*, 2517. (c) Babel, A.; Jenekhe, S. A. *Adv. Mater.* **2002**, *145*, 371. (d) Facchetti, A.; Deng, Y.; Wang, A.; Koide, Y.; Sirringhaus, H.; Marks, T. J.; Friend, R. H. *Angew. Chem., Int. Ed.* **2000**, *39*, 4547. (e) Facchetti, A.; Wang, A.; Marks, T. J.; Sirringhaus, H.; Deng, Y.; Friend, R. H. *Polym. Mater. Sci. Eng.* **2000**, *83*, 290. (f) Katz, H. E.; Johnson, J.; Lovinger, A. J.; Li, W. *J. Am. Chem. Soc.* **2000**, *122*, 7787.

(3) (a) Katz, H. E. *Chem. Mater.* **2004**, *16*, 4748. (b) Takimiya, K.; Kunugi, Y.; Toyoshima, Y.; Otsubo, T. *J. Am. Chem. Soc.* **2005**, *127*, 3605. (c) Takimiya, K.; Kunugi, Y.; Konda, Y.; Ebata, H.; Toyoshima, Y.; Otsubo, T. *J. Am. Chem. Soc.* **2006**, *128*, 3044. (d) Merlo, J. A.; Newman, C. R.; Gerlach, C. P.; Kelley, T. W.; Muyres, D. V.; Fritz, S. E.; Toney, M. F.; Frisbie, C. D. *J. Am. Chem. Soc.* **2005**, *127*, 3997. (e) Parkin, S. R.; Anthony, J. E.; Kuo, C.-C.; Jackson, T. N. *J. Am. Chem. Soc.* **2005**, *127*, 4986. (f) Xiao, K.; Liu, Y.; Qi, T.; Zhang, W.; Wang, F.; Gao, J.; Qiu, W.; Ma, Y.; Cui, G.; Chen, S.; Zhan, X.; Yu, G.; Qin, J.; Hu, W.; Zhu, D. *J. Am. Chem. Soc.* **2005**, *127*, 13281. (g) Ando, S.; Murakami, R.; Nishida, J. -I.; Tada, H.; Inoue, Y.; Tokito, S.; Yamashita, Y. *J. Am. Chem. Soc.* **2005**, *127*, 14996.

(4) Lin, Y. Y.; Gundlach, D. J.; Nelson, S. F.; Jackson, T. N. *IEEE Electron Device Lett.* **1997**, *18*, 87.

(5) Halik, M.; Klauk, H.; Zschieschang, U.; Schmid, G.; Ponomarenko, S.; Kirchmeyer, S. Weber, W. *Adv. Mater.* **2003**, *15*, 917.

(6) (a) Sundar, V. C.; Zaumseil, J.; Podzorov, V.; Menard, E.; Willett, R. L.; Someya, T.; Gershenson, M. E.; Rogers, J. *Science* **2004**, *303*, 1644. (b) Takeya, J.; Yamagishi, M.; Tominari, Y.; Hirahara, R.; Nakazawa, Y.; Nishikawa, T.; Kawase, T.; Shimoda, T.; Ogawa, S. *Appl. Phys. Lett.* **2007**, *90*, 102120. (c) Jurchescu, O. D.; Popinciuc, M.; van Wees, B. J.; Palstra, T. T. M. *Adv. Mater.* **2007**, *19*, 688.

10.1021/cm703499q CCC: $40.75
Published on Web 06/28/2008

Scheme 1. Chemical Structures of Pyrene Derivatives

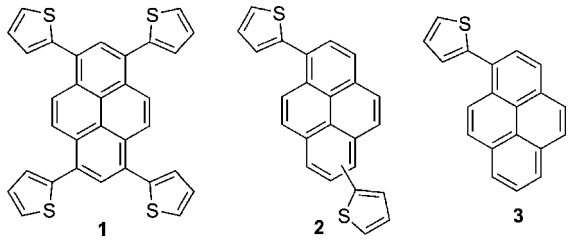

optimized molecular packing is indispensable. However, little is reported on such fundamental topics so far, despite the recent development of novel molecules and fabrication processes.[2,3] This would be because extrinsic effects from grain boundaries often obscure the intrinsic carrier transport properties of the polycrystalline organic materials in the commonly studied thin-film FETs. On the other hand, single-crystal OFETs are suitable for studies on the relevance of the molecular packing without complications due to the grain morphologies. Moreover, use of the single-crystal-based transistors expands the possibility of detecting the field effect even for low-mobility semiconductors which would not operate in the polycrystalline state.

In this study, we used molecules with the pyrene core because peripheral modifications can be easily accessible. Another advantage of the pyrene derivatives is that the crystals are favorably grown into the shape of thin platelets, so that their molecularly flat surface is utilized to form flat interfaces suitable for the FET channels as attached to the gate-insulating layer. In addition, the pyrene core is also a useful electroluminescent (EL) unit used in organic light-emitting FETs,[7] whose EL characteristics can be modified by peripheral modifications. We used the thienyl moiety as the peripheral groups (Scheme 1), expecting modified electron-donating and EL properties of pyrenes, and various molecular packings in the crystals. In this article, we report the synthesis, solution properties (redox, absorption, and emission), and crystal structures of pyrene derivatives (two isoforms of tetrathienyl pyrene **1**[8] and two isomers of dithienylpyrene **2**) and the FET performance based on their single crystals. We compare the FET performances of two isoforms or of two isomers with equivalent redox potentials, so that the involvement of molecular packing can be examined in the same conditions.

Experimental Section

General Remarks. All chemicals and solvents were of reagent grade unless otherwise indicated. All reactions were carried out under an argon atmosphere. THF was purified by distillation from sodium benzophenone kethyl under argon prior to use. Pyrene and monobromopyrene were purchased from Tokyo Casei Industry (TCI), and tetrabromopyrene **4** and dibromopyrene **5** were prepared according to previous reports.[9,10] NMR spectra were obtained with a JEOL JNM-AL300 spectrometer. UV−vis spectra were collected on a Shimazu 4121, and emission spectra were collected on a Shimazu 4123. Cyclic voltammetry (CV) was performed with an ALS electrochemistry analyzer model 610A. The measurement was performed in benzonitrile containing a donor molecule (0.2 mM) and tetra-*n*-butylammonium hexafluorophosphate (0.1 M) as a supporting electrolyte using a grassy carbon working electrode, platinum counter electrode, and $Ag/AgNO_3$ reference electrode. MS spectra were obtained with a JEOL JMS-SX102A for EI-MS. The melting points were determined with a Yanaco MP micromelting point apparatus. Microanalyses were performed at the Microanalysis Center, RIKEN.

Material Synthesis. *Tetrathienylpyrene* **1.** To a mixture of tetrabromopyrene (1.0 g, 1.93 mmol) and sodium carbonate (1.0 g) in 1,2-dimethoxyethane (20 mL) and water (30 mL) was added palladium tetrakistriphenylphosphine (0.082 g, 0.07 mmol) in one portion. The mixture was heated under reflux, and a solution of 2-thienylboronic acid (1.16 g 9.1 mmol) in 1,2-dimethoxyethane (20 mL) was added dropwise. The mixture was heated under reflux overnight and cooled. After removal of the solvent, the resulting residue was extracted with benzene and filtered through column chromatography (silica gel/benzene) to afford **1** as a pale yellow solid (0.25 g, 25%). Slow evaporation of the CS_2−hexane (1:1, v/v) solution and the physical vapor transport (PVT) method (detailed conditions are described in the FET Characteristics section) of **1** gave yellow needles suitable for X-ray analysis. Select data are identical to the previous report.[8] Compounds **2** and **3** were prepared similarly.

Dithienylpyrene **2.** Quantities were as follows: palladium tetrakistriphenylphosphine (0.041 g, 0.04 mmol), dibromopyrene (0.34 g, 0.94 mmol), and 2-thyenylboronic acid (0.36 g 2.8 mmol). Column chromatography (silica gel/CS_2) gave a pale yellow solid as a mixture of 1,6- and 1,8- isomers (71%). For X-ray analysis, slow evaporation of the CS_2−hexane (1:1, v/v) solution of **2** gave pale yellow needles of 1,8-isomer (*cis*-**2**), whereas the PVT method afforded pale yellow needles of 1,6-isomer (*trans*-**2**). Mp = 113−116 °C. ^{1}H NMR ($CDCl_3$): δ 7.23−7.28 (m, 6H), 8.07−8.21 (m, 6H), 8.49−8.52 (m, 2H). MS (*m*/*z*): 366 (M^+). Anal. Calcd for $C_{24}H_{14}$: C, 78.65; H, 3.85. Found: C, 78.27; H, 3.95. These spectra are for mixture of *cis*-**2** and *trans*-**2**.

Monothienylpyrene **3.** Quantities were as follows: palladium tetrakistriphenylphosphine (0.10 g, 0.09 mmol), monobromopyrene (0.80 g, 2.84 mmol), and 2-thyenylboronic acid (0.75 g 5.9 mmol). Flash column chromatography (silica gel/CS_2) gave white solid **3** (9%). Mp = 80−83 °C. ^{1}H NMR ($CDCl_3$): δ 7.27 (d, J = 3.7 Hz, 1H), 7.38 (dd, J = 2.2 Hz, J = 1 Hz, 1H), 7.52 (dd, J = 4.0 Hz, J = 1 Hz, 1H), 8.00−8.22 (m, 8H), 8.49 (d, J = 9.5 Hz 1H). MS (*m*/*z*): 284 (M^+). Anal. Calcd for $C_{20}H_{12}$: C, 84.47; H, 4.25. Found: C, 84.25; H, 4.25.

X-ray Crystal Structure Analysis. Crystal structures were determined by single-crystal X-ray diffraction data. Measurements were made on a Rigaku/MSC Mercury CCD system with graphite-monochromatized Mo Kα radiation (2μ < 55°). Structures were solved by direct methods (SIR97). Structures were refined by the full-matrix least-squares procedure by applying anisotropic temperature factors for all non-hydrogen atoms. The positions of the hydrogen atoms were calculated. The quality of the refined structures should be almost the same for the present samples since the *R* values are about 10%; therefore, the difference of FET performance would come from different molecular packings. The present crystal quality is sufficient with our estimation of overlap integrals in comparizon of FET performance. These values would

(7) Oyamada, T.; Uchiuzou, H.; Oku, Y.; Shimoji, N.; Matsushige, K.; Sasabe, H.; Adachi, C. *J. Appl. Phys.* **2005**, *98*, 074506−1.
(8) Zhang, H.; Wang, Y.; Shao, K.; Liu, Y.; Chen, S.; Qiu, W.; Sun, X.; Qi, T.; Ma, Y.; Yu, G.; Su, Z.; Zhu, D. *Chem. Commun.* **2006**, 755.
(9) Vollmann, H.; Becker, H.; Correll, M.; Streeck, H. *Justus Liebigs Ann. Chem.* **1937**, *531*, 1.
(10) (a) Grimshaw, J.; Trocha-Grimshaw, J. *J. Chem. Soc., Perkin* **1972**, *1*, 1622. (b) Minabe, M.; Takeshige, S.; Soeda, Y.; Kimura, T.; Tsubota, M. *Bull. Chem. Soc. Jpn.* **1994**, *67*, 172.

explain the difference of FET performance based on molecular packings discussed in the main text. Crystallographic data have been deposited at the CCDC, 12 Union Road, Cambridge CB2 1EZ, U.K., and copies can be obtained on request, free of charge, by quoting the publication citation and deposition numbers CCDC-668229-668232.

FET Characteristics. The single-crystal FETs were prepared by standard methods that were applied to copper phthalocyanine and rubrene crystal transistors.[11] Part of the single crystals of the pyrene-based compounds were grown by horizontal physical vapor transport (PVT) in a stream of argon gas;[12] using a two-zone tube furnace, powders of synthesized materials were sublimed in the upstream hot zone. The sublimed molecules were carried by an argon stream and crystallize in the downstream cold zone of the furnace. The temperatures of powder and crystal zones were kept typically for 12 h at 310 and at 280 °C, respectively. The rest were grown from solution in the CS_2−hexane (1:1, v/v) solution after recrystallizing twice to improve crystal quality. We selected thin crystals with a typical thickness of around 500 nm. The FET structure was composed by either attaching the crystals on substrates with polymeric gate insulators [poly(vinylphenol)] or depositing parylene through polymerization at room temperature.[11] Solartron 1260 and 1296 impedance analyzers were used to determine the capacitance of the gate dielectric insulators. We note that the two techniques were established using rubrene single crystals, giving equally high values of mobility exceeding 10 cm^2/V s. The transistor performances were measured using two source measure units (SMUs) equipped in an Agilent Technology E5270 semiconductor parameter analyzer; one applies gate voltage and the other applies drain voltage, and they measure drain current, so that the carrier conductivity in the semiconductor channel is measured as a function of the applied gate voltage.

Results and Discussions

Synthesis, Electrochemistry, and Optical Properties. The syntheses of the present compounds are outlined in Scheme 2. Synthesis of tetrathienylpyrene **1** was reported in ref 8. The starting tetrabromopyrene **4** and dibromopyrene **5** were prepared in a similar way to that described in previous reports.[9,10] The present compounds **1**, **2**, and **3** were prepared by ordinary Suzuki coupling reactions of bromo-substituted pyrene **4**, **5**, and **6** with 2-thienylboronic acid, respectively. Dibromopyrene **5**, which is almost a mixture of 1,6- and 1,8-dibromopyrene (ratio ≈ 5:4),[10] was used to yield a mixture of 1,6- and 1,8- isomers of **2**. To our knowledge, dithienylpyrene **2** and monothienylpyrene **3** were prepared for the first time.

Redox properties obtained by cyclic voltammetry (CV), UV absorption, and emission maximum values for the present compounds are summarized in Table 1 together with the corresponding data for pyrene for comparison. On the CV measurement, pyrene and **3** showed one quasi-reversible oxidation wave, while **1** and **2** showed two oxidation waves. The existence of the second step in **1** and **2** is ascribable to the widely spread π framework over peripheral thienyl groups. In particular, since a mixture of 1,6- and 1,8-isomers of **2** shows no distinct separation of the first oxidation step, the first oxidation potentials of 1,6- and 1,8-isomers of **2** should be almost the same. This is also confirmed by the extended Hückel calculation based on X-ray structure analysis which indicates almost the same HOMO level. The first oxidation potential decreases in the order pyrene > **3** > **2** > **1**, indicating the electron-donor ability is enhanced by introduction of the thienyl group. As expected, the absorption and emission maxima of a series of thienyl-substituted pyrenes are red shifted with increasing number of thienyl groups. These facts would indicate that the thienyl group reduces the energy separation between the highest occupied molecular orbital (HOMO) and the lowest unoccupied molecular orbital (LUMO) owing to the extended π conjugation.

Scheme 2. Synthesis of Thienyl-Substituted Pyrenes

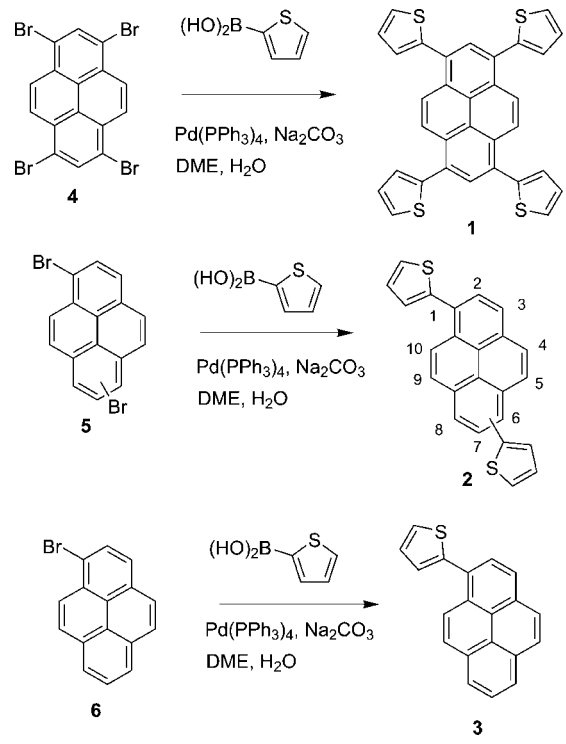

Table 1. Redox[a] and Photophysical[b] Properties

compounds	E^1_{ox} (V)	E^2_{ox} (V)	$\lambda_{abs,max}$ (nm)	$\lambda_{em,max}$ (nm)[c]
1	0.87	1.12	404	466
2[d]	0.96	1.12	372	434
3	1.14		349	405
pyrene	1.68		338	393

[a] Versus $Ag/AgNO_3$ in PhCN with 0.1 M n-Bu_4NPF_6, grassy carbon working electrode, scan rate 100 mV s^{-1}. [b] Measured in 10^{-5} M $CHCl_3$ solutions. [c] Excited at 315 nm for **1**, 293 nm for **2**, 278 nm for **3**, and 337 nm for pyrene. [d] A mixture of 1,6- and 1,8-isomers of **2**. In our measurement setup, errors in CV measurement are within 0.01 V.

Crystal Structures of Pyrene Derivatives. Single crystals of the pyrene derivatives were obtained by two different processes; one is slow evaporation from an organic solution, and the other is physical vapor transport (PVT). X-ray single-crystal structure analyses were carried out for **1** and **2**. Depending on crystallization methods, **1** afforded entirely different types of crystals: a monoclinic system with the

(11) (a) Podzorov, V.; Pudalov, V. M.; Gershenson, M. E. *Appl. Phys. Lett.* **2003**, *82*, 1739. (b) Takeya, J.; Goldmann, C.; Haas, S.; Pernstich, K. P.; Ketterer, B.; Batllogg, B. *J. Appl. Phys.* **2003**, *94*, 5800. (c) de Boer, R. W. I.; Klapwijk, T. M.; Morpurgo, A. F. *Appl. Phys. Lett.* **2003**, *83*, 4345. (d) Yamada, K.; Takeya, J.; Shigeto, K.; Tsukagoshi, K.; Aoyagi, Y.; Iwasa, Y. *Appl. Phys. Lett.* **2006**, *88*, 122110.
(12) Kloc, Ch.; Simpkins, P. G.; Siegrist, T.; Laudise, A. *J. Cryst. Growth* **1997**, *182*, 416.

Table 2. Crystallographic Data

	1a	**1b**	*cis*-**2**	*trans*-**2**
chemical formula	$C_{32}H_{18}S_4$	$C_{32}H_{18}S_4$	$C_{24}H_{14}S_2$	$C_{24}H_{14}S_2$
fw	530.73	530.73	366.49	366.49
color and shape	yellow needle	yellow needle	pale yellow needle	pale yellow needle
cryst syst	monoclinic	monoclinic	monoclinic	orthorhombic
space group	$P2_1/n$	P2/*n*	$P2_1/n$	*Pbca*
a (Å)	3.948(2)	14.192(14)	11.971(4)	7.88(1)
b (Å)	11.007(6)	6.135(5)	3.944(1)	11.44(2)
c (Å)	27.36(1)	15.912(17)	35.70(1)	18.11(3)
β (deg)	90.278(9)	116.158(16)	90.454(3)	
V (Å^3)	1188(1)	1243(2)	1685.4(9)	1631.3(3)
Z	2	2	4	4
D_{calcd} (g cm^{-3})	1.158	1.417	1.444	1.492
T (K)	297	297	297	297
R/R_w	0.1163/0.3397	0.1144/0.2415	0.0861/0.2644	0.1199/0.2969
reflns used	2711 ($I > 2.00\sigma$)	2833 ($I > 2.00\sigma$)	3838 ($I > 2.00\sigma$)	1871 ($I > 2.00\sigma$)

space group $P2_1/n$ by slow evaporation (**1a**) and a monoclinic system with the space group *P*2/*n* (**1b**) by the PVT method. Differential scanning calorimetry (DSC) measurement of **1** exhibited only one peak, suggesting that **1** does not have enantiotropic crystal polymorphism.[8] These structures are different from that reported previously (monoclinic, space group *C*2/*c*, $a = 20.664(4)$ Å, $b = 12.130(2)$ Å, $c = 14.363(3)$ Å, $\beta = 92.894(3)°$, $V = 3565.4(11)$ Å^3, $Z = 8$).[8] A mixture of 1,6- and 1,8-isomers of **2** afforded single crystals suitable for X-ray structure analysis: 1,8-isomer (abbreviated as *cis*-**2**) by slow evaporation and 1,6-isomer (abbreviated as *trans*-**2**) by the PVT method. However, we could not obtain single crystals of **3** for X-ray structure analysis. In this section, we report the molecular and crystal structures of the four crystals. In all samples, molecules contain a flat pyrene core connected to twisted thienyl rings. Crystallographic data for compounds **1a**, **1b**, *cis*-**2**, and *trans*-**2** are listed in Table 2.

Tetrathienylpyrene: 1a. The molecular and crystal structures of **1a** crystallized from a carbon disulfide−hexane solution are shown in Figure 1. **1a** crystallized in a monoclinic system with the space group $P2_1/n$. The molecule is located on an inversion center. The conformations of two crystallographically independent thienyl rings are twisted around the C2−C9 and C6−C13 bonds in the opposite directions. The torsion angles between the peripheral thienyl rings and the pyrene plane are 42.1(2)° for the C2−C9 bond and 41.7(2)° for the C6−C13 bond (Figure 1a). As shown in Figure 1b and 1c, the molecules make uniform stacks along the *a* axis and show cofacial overlap between adjacent molecules; the interplanar distance between the pyrene cores is 3.57(1) Å. The neighboring stacks are related to each other by the 2-fold screw symmetry along the *b* axis. There are no remarkable interstack short contacts within the sum of the van der Waals radii. Therefore, this structure seems to be one-dimensional, and sizable intermolecular overlap is expected only along the *a* axis. The intermolecular overlap integrals, *S*, between the HOMO based on the extended Hückel method are calculated to be $S_p \approx S_q \approx 2.5 \times 10^{-4}$ (energy dispersion of the present compounds is shown in Figure S1).[13] These *S* values result in no significant field effect for the single crystal of **1a** (vide infra).

(13) Mori, T.; Kobayashi, A.; Sasaki, Y.; Kobayashi, H.; Saito, G.; Inokuchi, H. *Bull. Chem. Soc. Jpn.* **1984**, *57*, 627.

Tetrathienylpyrene: 1b. The crystal of **1b** belongs to the monoclinic system with the space group *P*2/*n*. Figure 2 shows molecular and crystal structures of **1b**. As in **1a**, the molecule is located on an inversion center. The conformations of two crystallographically independent thienyl rings connected to C2 and C6 atoms are very similar to those in **1a** (Figure 2a); the torsion angles between the thienyl rings and the pyrene core are 47.5(5)° for the C2−C9 bond and

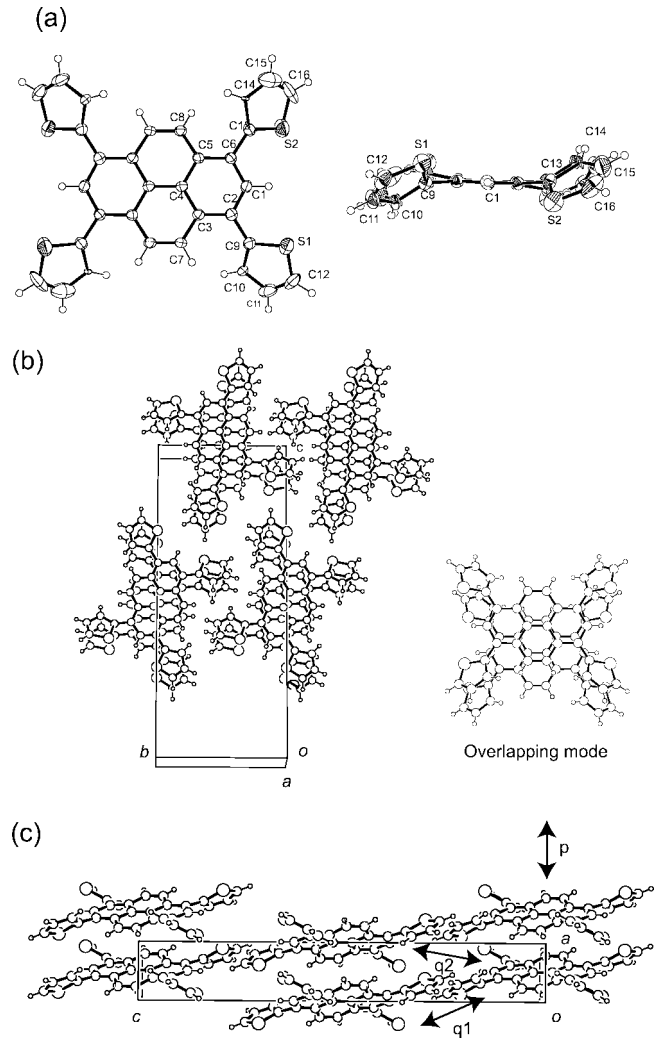

Figure 1. Crystal structures of **1a**. (a) Molecular structure, (b) projection on the *bc* plane (left) and overlapping mode (right), and (c) view along the *b* axis.

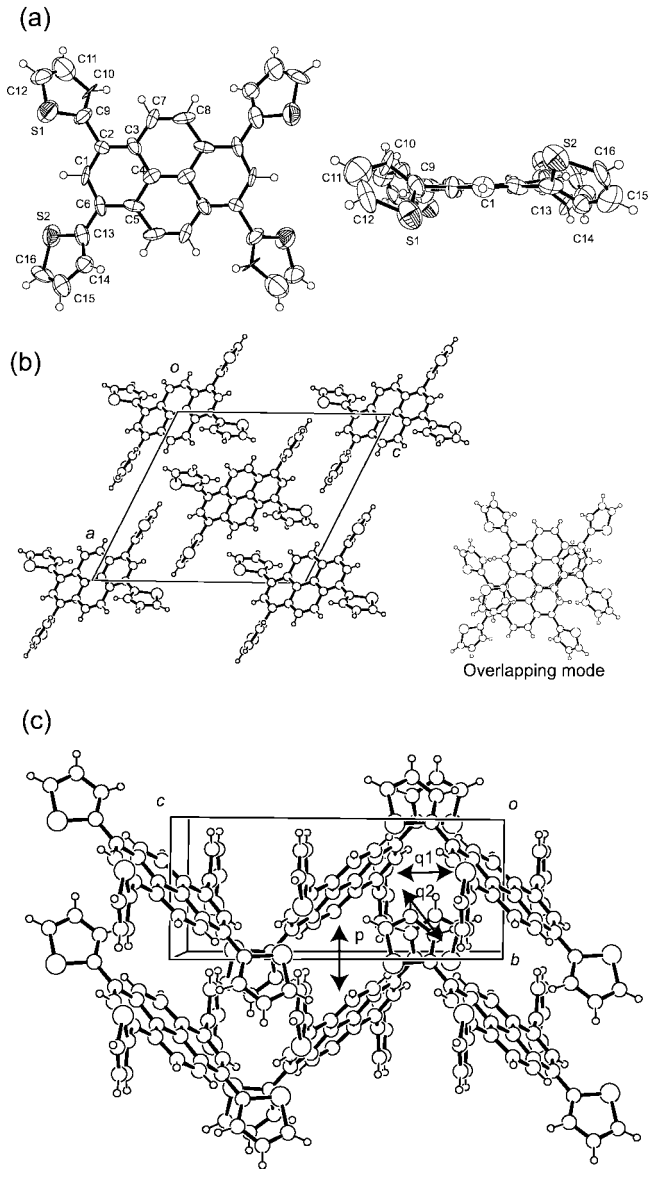

Figure 2. Crystal structure of **1b**. (a) Molecular structure, (b) projection on the *ac* plane (left) and overlapping mode (right), and (c) view along the *a* axis.

44.9(5)° for the C6−C13 bond. Although the inversion operation in **1a** and **1b** produces an analogous molecular geometry (planar pyrene core and twisted thienyl rings), it is noteworthy that a slight conformational (torsion angle) difference between the thienyl rings and the pyrene core would come from the molecular packing. As shown in Figure 2b and 2c, the molecules of **1b** uniformly stack along the *b* axis with an interplanar distance between the pyrene cores of 4.09(3) Å. The overlap integrals are $S_p = 1.3 \times 10^{-3}$, $S_{q1} = 1.1 \times 10^{-3}$, and $S_{q2} = 4.5 \times 10^{-5}$, which are significantly larger than those in **1a**. S_p in **1b** is 1 order of magnitude larger than those in **1a** despite the large interplanar distance in **1b** compared with that in **1a**. This points out that intermolecular $\pi-\pi$ interactions depend not only on the intermolecular distance but also on the intermolecular HOMO−HOMO phase relation. In the structure, these overlaps would be associated with CH···S contacts shorter than the van der Waals distance between the pyrene cores and the peripheral thiophene rings. The molecules in **1b** form conduction pathways in the *bc* plane.

Dithienylpyrene: *cis*-2. *cis*-**2** was crystallized in a monoclinic system with the space group $P2_1/n$ by slow evaporation from a CS_2−hexane solution. The molecular and crystal structures of *cis*-**2** are shown in Figure 3. As shown in Figure 3b, the molecules of *cis*-**2** make uniform stacks along the *b* axis; the interplanar distance between the pyrene cores is 3.58(1) Å. There is no side-by-side intermolecular contact in the structure. Therefore, *cis*-**2** has overlap integrals of $S_p = 2.5 \times 10^{-3}$ and $S_q = 7.0 \times 10^{-5}$, indicating the one-dimensional nature along the *b* axis. Since the single-crystal device made of this compound also works as an FET, it is likely that the overlap S_p is responsible for the FET operation (vide infra).

Dithienylpyrene: *trans*-2. The PVT method gave single crystals of the 1,6-isomer of **2** (*trans*-**2**) belonging to an orthorhombic system with the space group *Pbca*. The molecular and crystal structures of *trans*-**2** are shown in Figure 4. The C10/S1 and C13/S2 atoms of the thienyl ring are disordered (Figure 4a). In the crystal structure of *trans*-**2** there is no distinct stack, and the overlap integrals in *trans*-**2** are $S_p = 2.6 \times 10^{-4}$, $S_{q1} = 1.4 \times 10^{-3}$ $S_{q2} = 1.5 \times 10^{-3}$, and $S_{q3} = 2.2 \times 10^{-4}$. The overlap S_{q1} is associated with CH···S contacts shorter than the van der Waals distance between the pyrene cores and the peripheral thiophene rings, and the overlap S_{q2} comes from overlaps between neighboring thiophene rings. Among the positional disordered atoms of C10/S2 and S1/C13 (Figure 4a), the occupancy of S1 and C10 atoms is larger than that of S2 and C13 atoms. Therefore, S1 and C10 atoms are employed in the calculation of HOMO.

FET Characteristics. To examine the FET performances of the above compounds, we employed the single-crystal FET technique that has been recently developed.[11] Although we attempted crystal growth, the single crystal of **3** suitable for the FET measurement and X-ray structure analysis was not obtained. Figure 5a shows the top view of a typical single-crystal device for **1b** grown by the PVT technique. A platelet of a thin crystal of **1b** with a thickness of approximately 500 nm is *electrostatically laminated* to the substrate where source and drain electrodes are already implemented. The channel length L and width W are 150 and 100 μm, respectively. In the inset of Figure 5a the thin transparent crystal is elongated to the *b* axis direction and attached to two gold electrodes elongated in the direction of the *a* axis of the crystal. The overlapped regions work as source and drain electrodes. We note that the highest mobility of 40 cm^2/V s is achieved for rubrene single crystals, forming good ohmic contacts at the source and drain electrodes. The direction of the channel length is set parallel to the crystallographic direction with the largest orbital overlap for all the measured devices: the *a* axis for **1a**, the *b* axis for **1b**, the *b* axis for *cis*-**2**, and the *a* axis for *trans*-**2**. The direction of the single crystal was confirmed by X-ray structure analysis. The gate insulators used were poly(vinylphenol) for **1a** and **1b** and for parylene *cis*-**2** and *trans*-**2**, respectively.

Plotted in Figure 5a are transfer characteristics of the single-crystal devices of the two tetrathielyl isoforms **1a** and

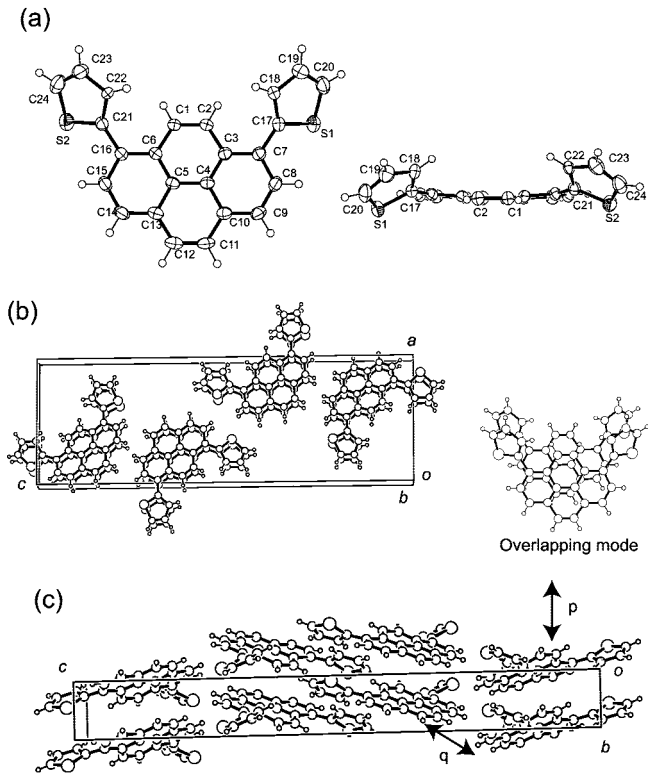

Figure 3. Crystal structure of *cis*-**2**. (a) Molecular structure, (b) projection on the *ac* plane (left) and overlapping mode (right), (c) view along the *a* axis.

1b. The device of **1b** shows apparent *p*-type field-effect characteristics as negative gate voltage V_G is applied; the drain current I_D (driven by the drain voltage V_D) increases with mobile holes accumulated at the surface of the single crystal. The FET mobility is estimated to be $\mu \approx 0.02$ cm^2/V s using the standard equation $\mu = L/W \cdot 1/(C_i V_D) \cdot dI_D/dV_G$, where C_i is the capacitance of the gate insulator. Typical output characteristics shown in Figure 5b are obtained for the same device of the **1b** crystal, giving almost the same value of saturation mobility. We note that the presented data are of the device with the highest mobility among five samples. Except for the one with an apparently badly laminated crystal, all the other devices showed field effect with mobilities in the range of 0.005−0.02 cm^2/V s in which the distribution could be related to influences of interfacial traps underneath the thin crystals.

On the other hand, none of three devices based on single crystals of the same compound **1a** show any indication of the field effect. In our setup, it means that the mobility value is less than $\sim 10^{-5}$ cm^2/V s, if any. Even with the highest mobility 0.02 cm^2/V s of **1b** crystal devices it is difficult to assume band transport because the mean free path is estimated roughly 2 orders of magnitude shorter than the typical molecular distance. (We indeed experienced that the mobility decreased at a colder atmospheric temperature.) Therefore, the carrier transport mechanism is most likely due to hopping. Regarding the well-known semiclassical Marcus theory, the rate for the carrier hopping k is described by representative overlap integral S and the reorganization energy μ which references geometric relaxation of the charged molecules;

$$k = \frac{4\pi^2}{h} \cdot \frac{S^2}{\sqrt{4\pi\lambda T}} \cdot e^{\frac{-\lambda}{4k_B T}} \quad (1)$$

where h and k_B are Plank's constant and Boltzmann's constant, respectively. Noting that the component molecules of the two crystals are exactly the same, the reorganization energy is identical between the two isoform crystals. Therefore, the essential difference in mobility is attributed to the variation in the molecular packing of the crystals. As discussed above, crystallographic analysis shows intermolecular overlaps of about 10^{-3} for the **1b** crystal, whereas the value of the primary overlap integral is one order of magnitude smaller for the **1a** crystal. Therefore, it can be inferred from eq 1 that the difference in S can cause the difference in the transistor performances between the two isoforms.

Next, we compare the field-effect performances for the crystals of isomer compounds *cis*-**2** and *trans*-**2**. These two molecules have the same number of the thienyl groups and

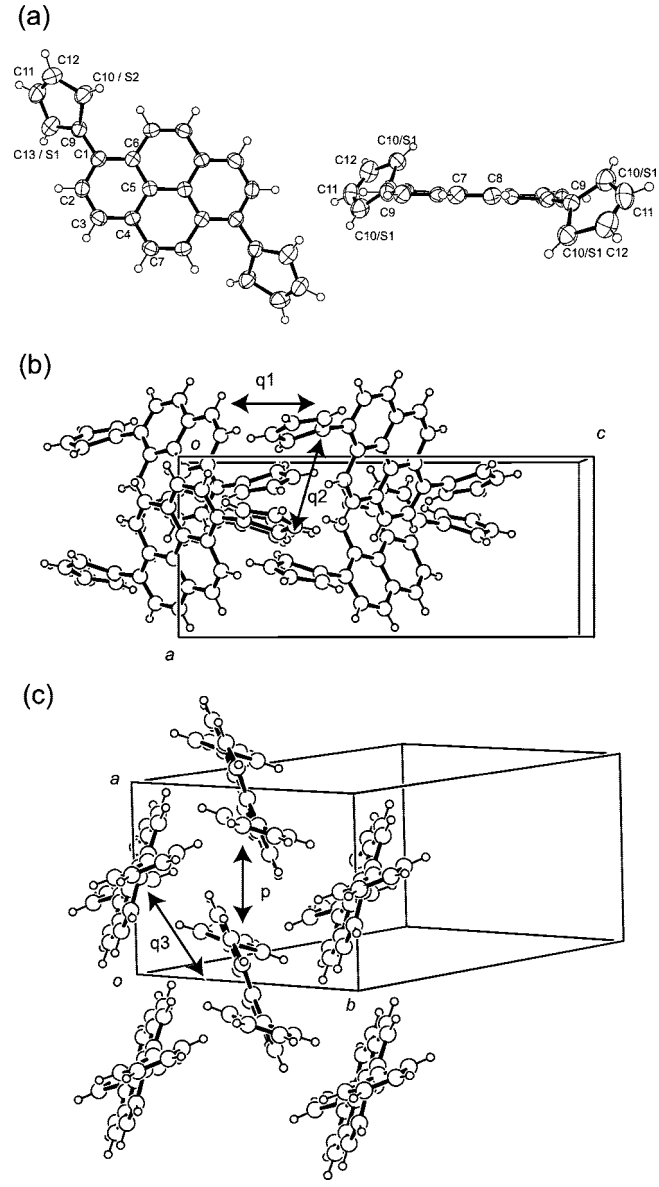

Figure 4. Crystal structure of *trans*-**2**. (a) Molecular structure, C10/S1 represents the positional disorder, (b) projection on the *ac* plane, and (c) projection on the *ab* plane.

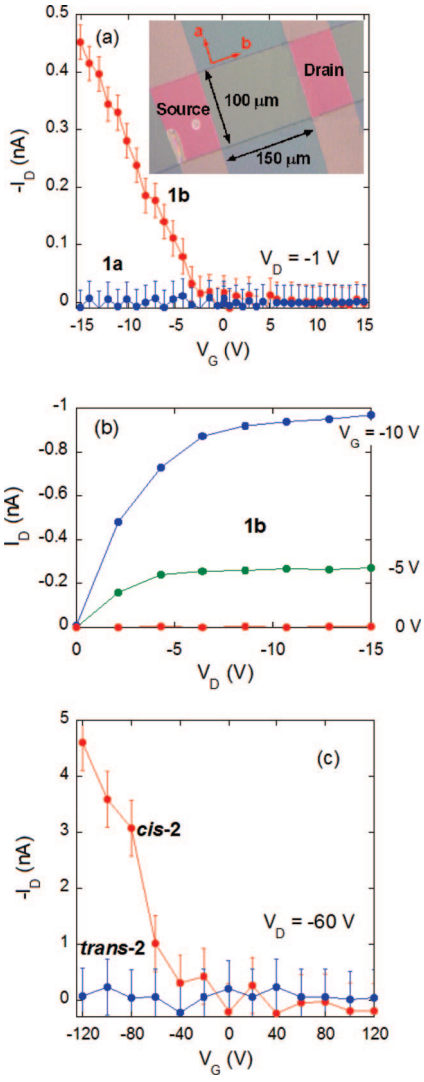

Figure 5. (a) Transfer characteristics of the **1a** and **1b** transistors. (b) Output characteristics of the **1a** transistors. (c) Transfer characteristics of the *cis*-**2** and *trans*-**2**.

similar electron-donor ability as indicated by the CV measurement and the extended Hückel calculation but exhibit different molecular packing patterns. Figure 5c shows the transfer characteristics of the devices of the two single crystals. The results show that the *cis*-**2** device works as an FET with a mobility value of 10^{-4} cm^2/V s. All three *cis*-**2** devices exhibit mobility higher than 0.5×10^{-4} cm^2/V s, whereas none of the *trans*-**2** devices show field effect. Again, we can attribute the difference in the FET performance to the crystal packing; the *cis*-**2** crystal has orbital overlap larger than those of the *trans*-**2** crystal. We note that a working transistor is obtained for the dithienyl crystals grown from a solution, while the tetrathienyl crystals grown by the PVT method exhibit the apparent FET performance. Therefore, the method of crystallization is not the predominant factor to determine the FET performance in the present crystals.

A comparison between the *cis*-**2** crystal and the **1b** crystal indicates that the mobility values differ by two orders though the overlap integrals are in the same order, suggesting that two-dimensional overlaps in **1b** are more effective for carrier transport than one-dimensional overlaps in *cis*-**2**. As for different threshold voltages, the different gate insulators would be related. Since the results of the CV measurements indicate a stronger electron-donor ability for the tetrathienyl compound (small mismatch with Au work function), a lower Schottky barrier at the source electrode results in a higher hole-injection rate in the **1b** crystal, providing a possible reason for the higher carrier transport in the **1b**.

The present experiment also gives an implication for the least electronic intermolecular coupling to provide the FET operation. Within the series of crystals of molecular compounds of identical conjugated orbitals of pyrene, those with overlap integrals on the order of 10^{-3} shows apparent FET characteristics, even though the different extent of contribution of interface traps causes the variation in mobility values. On the other hand, none of the single-crystal transistors based on compounds with integrals smaller than 10^{-4} show the carrier transport. It appears that the lower limit for OFET operation resides in the range of $S \approx 10^{-4}-10^{-3}$, which corresponds to a transfer integral $t \approx 10^{-3}-10^{-2}$ eV. Since the energy scale is one order smaller than that of room temperature, the electronic system cannot realize band transport without a well-defined Fermi surface. On the other hand, the overlap integrals in the pentacene crystal[14] widely used in high-performance FET both in single crystal and thin film form are approximately larger than that of the present molecules (intrastack, -1.6 and -1.8×10^{-3}; interstack, 2.6 and -3.8×10^{-3}) and show two-dimensional nature. Also, rubrene, which shows the highest mobility in the form of the single-crystal transistors, has almost the same size of overlap integrals. The present molecules are different from pentacene in view of electronic properties. However, this implies that not only magnitude but also dimensionality of the intermolecular overlaps are predominant factors for carrier transport even if the channel of FET is set parallel to the largest intermolecular overlap. Since band transport is realized in these materials, as recently evidenced by Hall-effect measurements of rubrene single-crystal transistors,[15] these high-mobility semiconductors are apparently in a different class as compared to the series of pyrene derivatives. The present observation indicates that the overlap integrals are still linked to the carrier mobility through such mechanisms as given in eq 1, giving rise to the minimum orbital overlap for the field-effect operation that depends on molecular reorganization.

Conclusion

A series of pyrene derivatives with peripheral thienyl groups have been synthesized to study field-induced carrier transport as semiconductors in organic transistors. Application of the organic single-crystal FET technique has revealed the transport properties intrinsic to the materials with regard to the molecular packing. Direct comparisons between the two isoforms of tetrathienylpyrene and between the two isomers of dithienylpyrene demonstrate that larger overlap integrals between the adjacent molecules favor the FET

(14) Mattheus, C. C.; Dros, A. B.; Baas, J.; Meetsma, A.; Boer Jan, L.; de; Palstra, T. T. M. *Acta Crystallogr.* **2001**, *C57*, 939.
(15) (a) Takeya, J.; Tsukagoshi, K.; Aoyagi, Y.; Takenobu, T.; Iwasa, Y. *Jpn. J. Appl. Phys.* **2005**, *46*, L1393. (b) Podzorov, V.; Menard, E.; Rogers, J. A.; Gershenson, M. E. *Phys. Rev. Lett.* **2005**, *95*, 226601.

performances. It has turned out that the molecular packing is relevant even in the absence of the apparent band transport for the poorly overlapped molecules and that the transfer integral critical for the FET operation is in the range of $10^{-3}-10^{-2}$ eV for the series of the pyrene derivatives. The present experiment has demonstrated an advanced evaluation using single-crystal transistors for designing new molecules toward high-performance organic semiconductors.

Acknowledgment. We thank Dr. Takeo Minari (RIKEN), Dr. Kazuhito Tsukagoshi (RIKEN), and Dr. Masafumi Tamura (RIKEN) for critical comments and discussions. This work was partially supported by a Grant-in-Aid for Scientific Research (Nos. 16GS0219, 17069003, 18028029, and 19360009) from the Ministry of Education, Culture, Sports, Science, and Technology of Japan. It was also partially supported by Industrial Technology Research Grant Program in 2006 from the New Energy and Industrial Technology Developing Organization (NEDO) of Japan.

Supporting Information Available: X-ray data in CIF format and energy band structures for **1a**, **1b**, *cis*-**2**, and *trans*-**2** (PDF). This material is available free of charge via the Internet at http://pubs.acs.org.

CM703499Q